JOC The Journal of Organic Chemistry

Note

pubs.acs.org/joc

A Mechanistic Study on the Amidation of Esters Mediated by Sodium Formamide

Antonio Ramirez,* Boguslaw Mudryk, Lucius Rossano, and Srinivas Tummala

Chemical Development, Bristol-Myers Squibb Company, One Squibb Drive, New Brunswick, New Jersey 08903, United States

Supporting Information

ABSTRACT: Kinetic and computational studies on the amidation of esters with mixtures of formamide and sodium methoxide are described. Rate studies are consistent with a fast deprotonation of formamide followed by two reversible acyl transfers affected by solvent participation. MP2 calculations suggest that the first acyl transfer between the ester and sodium formamide is rate-determining. The transition structures leading to the formation and collapse of the first tetrahedral intermediate are calculated to be isoenergetic.

The amidation of esters using formamide and sodium methoxide is a procedure commonly used for the preparation of carboxamides in industrial[1] and academic[2] syntheses. More than four decades ago, Allred and Hurwitz at Rohm and Haas published the first and so far only mechanistic examination of this reaction based on a series of control experiments. Although at that time the complexity of the transformation prevented detailed studies, the authors concluded that the amidations consist of a sequence of reversible steps that include *N*-acylformamides as intermediates.[3] A generic sequence for the amidation shown in eqs 1 and 2 involves (i) formamide deprotonation by sodium methoxide (MeONa), (ii) acyl transfer from ester **1** to sodium formamide to afford the intermediate sodium *N*-acylformamide **2**, and (iii) formyl transfer from *N*-acylformamide **2** to formamide to generate amide **3** and sodium diformylamide.

$$HCONH_2 + MeONa \rightleftharpoons HCONHNa + MeOH \quad (1)$$

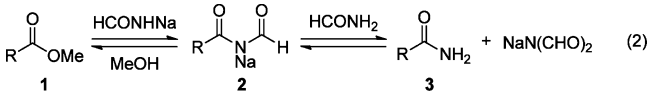

During the development of the oral anticoagulant Apixaban[4] (**6**, Scheme 1), we were compelled to gain further insights into the key amidation step in order to optimize the reaction outcome and build a predictive kinetic model.[5] Of central interest to the process team was the evaluation of critical kinetic and thermodynamic parameters to enable optimal control of reaction rates and yields. Herein we report mechanistic studies that shed light on the underlying complexities of the ester amidation promoted by sodium formamide.

We began investigating the MeONa-mediated deprotonation of formamide in DMF (eq 1).[6] The use of a ReactIR system allowed us to monitor the disappearance of formamide (1710 cm^{-1}) and concomitant formation of its sodium salt (1580 cm^{-1}).[7] The deprotonation occurred instantaneously upon addition of MeONa at 0 °C[8] to afford $K_{eq} = 25 \pm 5$, indicating that under the reaction conditions (24 equiv of formamide relative to MeONa) sodium formamide is the major sodium-bearing species in solution (>99.8 mol %).[9] Next, we explored

Scheme 1. Ester Amidation via Sodium *N*-Acylformamide 5

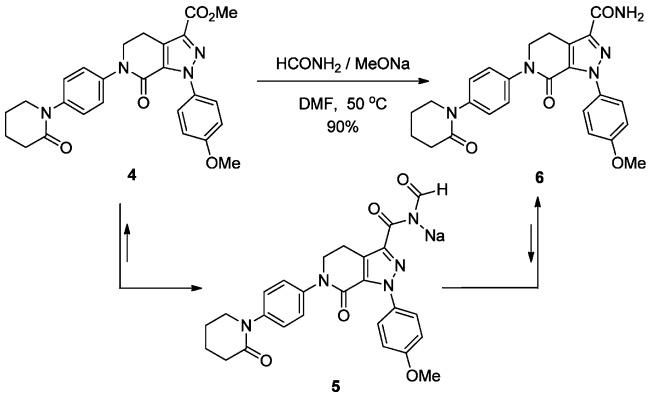

the equilibria generally represented in eq 2 by completing a sequence of control experiments. Reaction of carboxamide **6** in the absence of formamide with excess sodium diformylamide[10] in DMF/MeOH afforded mixtures of carboxamide **6** and ester **4** with [**6**]/[**4**] ratios that decreased at higher concentrations of added sodium diformylamide (Figure 1a). Submission of the protonated form of *N*-acylformamide **5** to the reaction conditions resulted in instantaneous conversion to give mixtures of carboxamide **6** and ester **4** with increasing [**6**]/[**4**] ratios at higher formamide/MeOH proportions (Figure 1b). These observations support a reversible amidation that requires excess formamide to promote the formation of carboxamide **6**.

Kinetic studies on the amidation of ester **4** were performed using the method of initial rates[11] in the presence of excess sodium formamide and formamide relative to MeOH to effectively trap *N*-acylformamide **5**. HPLC analyses of the reaction mixtures revealed a clean decay of ester **4** and simultaneous formation of carboxamide **6** along with trace amounts of the steady-state intermediate **5** in isolated

Received: October 21, 2011
Published: November 16, 2011

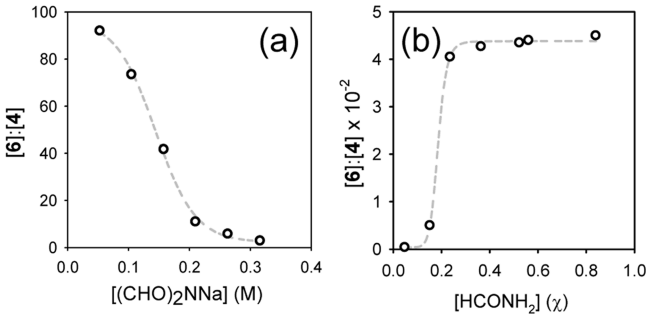

Figure 1. (a) Plot of [**6**]/[**4**] molar ratios versus [$(CHO)_2NNa$] for the conversion of carboxamide **6** (0.011 M) to ester **4** in 6.5 M DMF/MeOH after 24 h at 20 °C. (b) Plot of [**6**]/[**4**] ratios versus formamide mole fraction (χ) for the reaction of *N*-acylformamide **5** (0.010 M) with MeONa (0.67 M) in formamide/MeOH mixtures after 24 h at 20 °C.

experiments.[12] A kinetic isotope effect k_H/k_D = 1.4 ± 0.1 determined by comparing amidations in formamide/MeOH and formamide-d_3/MeOD mixtures is consistent with solvent participation in the reaction coordinate. Monitoring the decay of **4** over a range of substrate, sodium formamide, formamide, and MeOH concentrations using DMF as the cosolvent affords first-order dependencies in substrate and sodium formamide along with saturation kinetics in formamide and MeOH (Figure 2). Within the saturation regime in solvent, the reaction orders are consistent with the rate law in eq 3 and the general rate-determining step in eq 4, where *m* denotes the aggregation state of sodium formamide, *S* represents the coordinating solvents, and *n* defines the solvation number.[13] The rate dependencies at low MeOH and formamide concentrations will be discussed in the context of computational studies below.

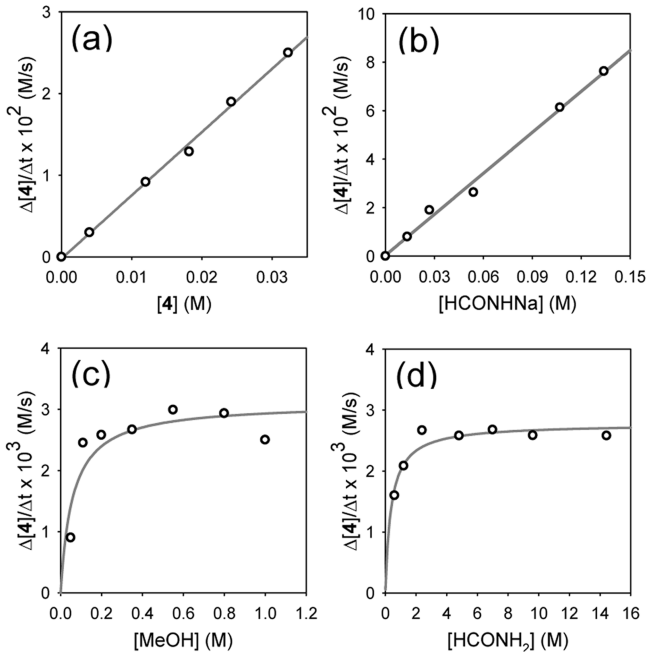

Figure 2. Plots of initial rates for the amidation of ester **4** by HCONHNa at 0 °C versus (a) [**4**], (b) [HCONHNa], (c) [MeOH], (d) [$HCONH_2$]. Rate dependencies on [**4**] and [HCONHNa] were measured in [MeOH] = 0.46 M and [$HCONH_2$] = 4.8 M. Rate dependencies on [MeOH] and [$HCONH_2$] were measured using [**4**] = 0.004 M and [HCONHNa] = 0.027 M in [$HCONH_2$] = 4.8 M and [MeOH] = 0.11 M, respectively. Additional data are included in Supporting Information.

$$\text{rate} = k'[\mathbf{4}]^1[\text{HCONHNa}]^1[\text{MeOH}]^0[\text{HCONH}_2]^0 \quad (3)$$

$$[(\text{HCONHNa})_m\text{S}_n] + \mathbf{4} \rightarrow [(\text{HCONHNa})_m\text{S}_n(\mathbf{4})]^{\neq} \quad (4)$$

A Hammett plot for the analogous amidation of *p*-substituted methyl benzoates gives ρ = 2.2 ± 0.3, indicating the transfer of negative charge from sodium formamide to ester **4** in the rate-determining transition state.[14]

We investigated the amidation of model substrate **7** using DFT calculations at the B3LYP/6-31+G(d) level of theory. A series of geometries were tested for reactants, intermediates, and transition structures, and the optimized structures were submitted to single-point MP2/6-31+G(d) calculations incorporating thermal corrections to Gibbs free energy as obtained from the frequency analysis at the B3LYP/6-31+G(d) level and PCM corrections for formamide as the solvent (ΔG, 298.15 K, 1.0 atm).[15] Admittedly, the choice of implicit solvation and monomeric sodium formamide to simplify the unattainable combination of aggregates and solvates provides results that must be interpreted with caution. The discussion will focus on three aspects: (i) the deprotonation of formamide, (ii) the nature of the rate-determining transition structure, and (iii) the evaluation of the kinetically obscure formyl transfer.

The computational study of the reaction between MeONa and formamide reveals a barrierless and exothermic deprotonation (ΔG = −5.5 kcal·mol^{-1}), in agreement with experimental results (Scheme 2). Transition structure **TS1** displays an optimal geometry for the proton transfer with a planar six-membered ring and a virtually linear N−H−O angle.[16]

Scheme 2. MP2/6-31+G(d) Energies for the Deprotonation of Formamide by MeONa (ΔG, kcal·mol^{-1})

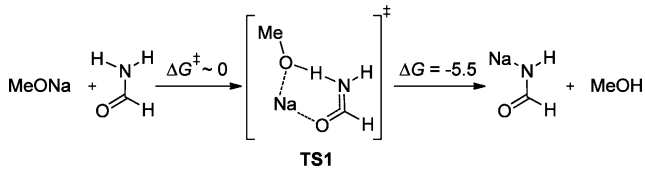

The lowest energy pathway calculated for the reaction between sodium formamide and ester **7** is summarized in Figure 3. The calculations depict a slightly exothermic conversion (ΔG = −1.0 kcal·mol^{-1}) involving transition structures of comparable activation energies (~1.5 kcal·mol^{-1}), the first acyl transfer between sodium formamide and ester **7** to give *N*-acylformamide **9** is rate-determining. However, the calculations are not able to distinguish between the addition of sodium formamide to ester **7** (**TS2**) and the elimination of MeOH from tetrahedral intermediate **8** (**TS3a**) because both transitions states exhibit identical activation energies ($\Delta G^{\ddagger}$ = 23.2 kcal·mol^{-1}).[17] The assistance of a molecule of formamide in **TS3a** reduces the activation energy for the C(O)−OMe bond cleavage relative to the uncatalyzed pathways **TS3b** and **TS3c**, the MeOH-mediated cleavage **TS3d**, and the direct elimination of basic MeONa in **TS3e**[18] (Figure 4). Presumably, formamide stabilizes the departure of the −OMe leaving group

dx.doi.org/10.1021/jo2021828 | J. Org. Chem. 2012, 77, 775−779

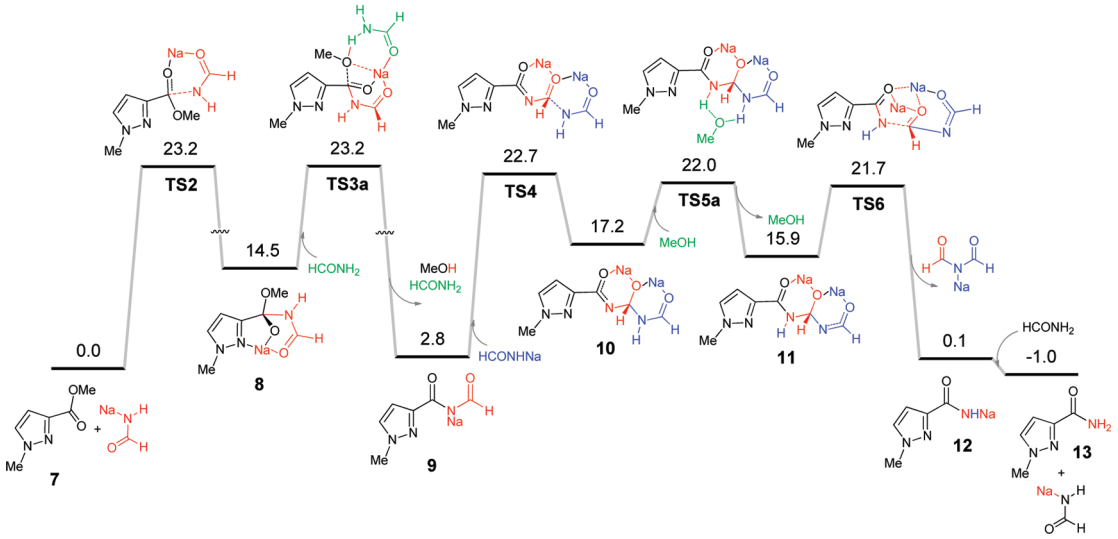

Figure 3. Lowest energy pathway calculated for the amidation of ester **7**. MP2/6-31+G(d) energies include thermal corrections to Gibbs free energies and a PCM solvent model for formamide (ΔG, kcal·mol^{-1}).

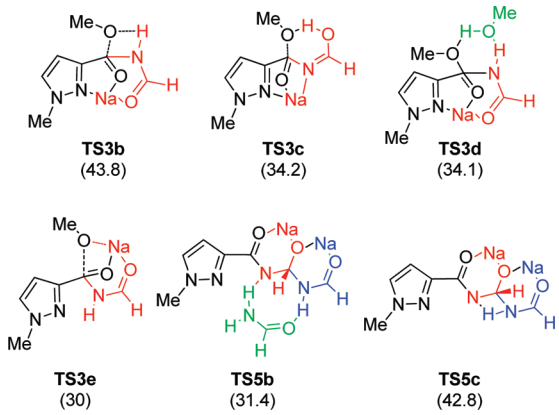

Figure 4. Alternative transition structures **TS3** and **TS5**. Calculated activation energies ($\Delta G^{\ddagger}$, kcal·mol^{-1}) are given in parentheses.

in a process followed by the barrierless regeneration of sodium formamide and deprotonation of the resulting *N*-acylformamide.[19] Allred and Hurwitz proposed the nucleophilic attack of MeONa to the protonated form of *N*-acylformamide **9** as the next step in the sequence.[3] However, two simple observations challenge this proposal. First, the higher acidity of the conjugated acid of *N*-acylformamide **9** relative to formamide and MeOH determines its overwhelming existence as the sodium salt **9**.[20] Second, the virtually complete deprotonation of formamide by MeONa results in a negligible concentration of MeONa. Taken together, these observations suggest the prevalence of a formyl transfer from sodium *N*-acylformamide **9** to sodium formamide. The examination of the nucleophilic attack of sodium formamide to sodium *N*-acylformamide **9** affords **TS4** along with tetrahedral intermediate **10**. Subsequently, **10** undergoes a 1,3-proton shift to give isomer **11**.[21] The most stable transition structure (**TS5a**) for the conversion of **10** to **11** includes a molecule of MeOH as the proton shuttle between the two amide nitrogens. Attempts to locate transition structures corresponding to the participation of formamide as the proton shuttle (**TS5b**) or a direct 1,3-proton shift (**TS5c**) resulted in structures with lower stabilities possibly due to the poor ability of formamide to transfer a proton between two heteroatoms[22] and the inadequate geometric arrangement in the four-membered ring,[16] respectively (Figure 4). Tetrahedral intermediate **11** displays a lengthened N(H)−C(O) bond (1.51 Å) relative to isomer **10** (1.45 Å) en route to its cleavage through **TS6**. Finally, deprotonation of formamide by the resulting sodium carboxamide **12** is moderately favored to afford the desired carboxamide **13** and sodium formamide.

The participation of formamide during the departure of the −OMe group in **TS3a** is seemingly at odds with the experimental zeroth-order dependence observed at high formamide concentrations (Figure 2d).[23] The existence of the sodium formamide reactant as a formamide solvate would offer a plausible explanation for the discrepancy. Indeed, a saturation behavior for the formation of sodium formamide−formamide complexes in DMF/MeOH mixtures (eq 5) is in agreement with reports that indicate a coordinating ability for sodium salts that follows the order formamide ≥ DMF > MeOH.[24] The persistence of such a complex in transition state **TS3a** would concur with the observed first-order in sodium formamide and zeroth-order in formamide at concentrations higher than 2 M (eq 6). In contrast, the saturation behavior in MeOH could be traced to the requirement of sufficient MeOH to facilitate the 1,3-proton shift in **TS5a**, which in the absence of MeOH would be rate-determining (**TS5b** or **TS5c**).

$$[(\mathrm{HCONHNa})_m\mathrm{DMF}_o] + n(\mathrm{HCONH_2}) \rightleftharpoons [(\mathrm{HCONHNa})_m(\mathrm{HCONH_2})_n] + o(\mathrm{DMF}) \quad (5)$$

$$[(\mathrm{HCONHNa})_m(\mathrm{HCONH_2})_n] + \mathbf{4} \rightarrow [(\mathrm{HCONHNa})_m(\mathrm{HCONH_2})_n(\mathbf{4})]^{\neq} \quad (6)$$

In summary, kinetic and computational studies depict the amidation of esters with sodium formamide as a multistep sequence that involves two reversible acyl transfer reactions. MP2/6-31+G(d) energies suggest that the first acyl transfer between the ester and sodium formamide corresponds to the highest energy barrier within the sequence. The second acyl transfer step takes place via an unusual exchange of the formyl group between two ion pairs.

In a more general overview, we performed these studies prompted by the need to provide the kinetic and equilibrium

dx.doi.org/10.1021/jo2021828 | *J. Org. Chem.* 2012, 77, 775−779

data required to build a mechanistic model. Such a model had to reproducibly and reliably predict both the observed reaction rates and the varying final levels of ester **4**, sodium *N*-acylformamide **5**, and carboxamide **6** under a broad range of experimental conditions. The investigations that resulted in the delivery of a quality by design regulatory filing for Apixaban have been recently discussed elsewhere.[25]

EXPERIMENTAL SECTION

General Information. DMF, formamide, and MeOH >99.8% pure by GC analysis were dried over molecular sieves and their water contents determined by coulometric Karl Fischer titration (H_2O <0.005%). MeONa stock solutions in dry MeOH were titrated for active base using literature methods.[26] Sodium diformylamide was purified by recrystallization from toluene. All of the materials were manipulated under nitrogen using standard vacuum line and syringe techniques. All reactions were performed under an inert atmosphere of dry nitrogen in 20 mL oven-dried vials fitted with TFE septa. Gas-tight syringes were used to transfer moisture-sensitive solutions. Reaction samples quenched with 1:1 H_2O–ACN were analyzed on a HPLC system equipped with a C8 column (4.6 × 50 mm) and a SPD-20A/20AV UV–vis detector. The relative response factors of compounds **4**, **5**, and **6** measured at 280 nm are 1.00 ± 0.01. ^{1}H NMR and ^{13}C NMR spectra were recorded on a 400 MHz spectrometer in $CDCl_3$ unless stated otherwise. Chemical shifts for ^{1}H and ^{13}C NMR spectra are reported in parts per million downfield from TMS. NMR data are represented as follows: chemical shift (δ, ppm), multiplicity (s = singlet, d = doublet, t = triplet, m = multiplet), coupling constants (J, Hz), and integration. Infrared spectra were obtained in CH_2Cl_2 using a ReactIR fitted with a Sentinel probe within a spectral range of 4000–650 cm^{-1}.

Preparation of Methyl 1-(4-Methoxyphenyl)-7-oxo-6-[4-(2-oxo-1-piperidinyl)phenyl]-4,5,6,7-tetrahydro-1*H*-pyrazole-[3,4-*c*]pyridine-3-carboxylate (4). A 25% by weight solution of MeONa in MeOH (0.8 mL, 3.5 mmol) was added to a solution of the ethyl ester analogue of **4**[4c] (1.0 g, 2.0 mmol) in DMF (8 mL). The reaction mixture was heated to 50 °C for 1 h and cooled to rt before the addition of TFA (0.33 mL) and water (15 mL). The resulting precipitate was filtered, washed with 3 × 10 mL of water, 1 × 10 mL of MTBE, and dried to afford the desired methyl ester **4** as a white solid (0.76 g, 78%): HPLC purity >99%; IR (CH_2Cl_2) 1722, 1676, 1646 (C═O) cm^{-1}; ^{1}H NMR (400 MHz, $CDCl_3$) δ 7.47 (d, J = 9.3 Hz, 2H), 7.35 (d, J = 9.1 Hz, 2H), 7.26 (d, J = 9.1 Hz, 2H), 6.91 (d, J = 8.8 Hz, 2H), 4.13 (t, J = 6.6 Hz, 2H), 3.98 (s, 3H), 3.81 (s, 3H), 3.59 (t, J = 6.2 Hz, 2H), 3.32 (t, J = 6.6 Hz, 2H), 2.55 (t, J = 5.6 Hz, 2H), 1.93 (m, 4H); ^{13}C NMR (100 MHz, $CDCl_3$) δ 169.8, 162.0, 159.5, 156.7, 141.0, 139.5, 138.3, 132.7, 132.1, 126.5, 125.8, 113.2, 55.1, 51.7, 51.2, 50.6, 32.4, 23.1, 21.0, 20.9; HRMS (ESI) calcd for $C_{26}H_{27}N_4O_5$ [M + H$^+$] 475.1981, found 475.1961.

Preparation of *N*-Formyl 1-(4-Methoxyphenyl)-7-oxo-6-[4-(2-oxo-1-piperidinyl)phenyl]-4,5,6,7-tetrahydro-1*H*-pyrazole-[3,4-*c*]pyridine-3-carboxamide (Protonated Form of Intermediate 5). A solution of carboxamide **6** (0.5 g, 1.1 mmol) in DMF–dimethyl acetal (4 mL, 27 equiv) was heated to 120 °C under nitrogen for 10 min. After cooling the solution to rt, 10 mL of acetic acid (70% by volume, aqueous solution) was added and the resulting mixture was stirred at rt for 18 h to give a precipitate. This precipitate was collected, washed with water (6 mL), and dried in vacuo to provide a white solid (0.38 g, 72%): IR (CH_2Cl_2) 3370 (NH), 1737, 1700, 1677, 1646 (C═O) cm^{-1}; ^{1}H NMR (400 MHz, $CDCl_3$) δ 9.40 (m, 2H), 7.47 (m, 2H), 7.26 (m, 4H), 6.94 (m, 2H), 4.13 (t, J = 6.6 Hz, 2H), 3.83 (s, 3H), 3.60 (m, 2H), 3.36 (t, J = 6.6 Hz, 2H), 2.55 (t, J = 5.9 Hz, 2H), 1.93 (m, 4H); ^{13}C NMR (100 MHz, $CDCl_3$) δ 169.9, 161.2, 160.8, 159.9, 156.6, 141.4, 139.4, 138.5, 133.9, 131.8, 126.8, 126.6, 126.4, 125.9, 113.5, 55.3, 51.3, 50.7, 32.6, 23.3, 21.1, 20.9; HRMS (ESI) calcd for $C_{26}H_{25}N_5O_5$ [M + H$^+$] 488.1928, found 488.1925.

IR Titration Experiments. IR spectra were recorded using a ReactIR spectrometer fitted with an 18-bounce silicon-tipped probe. The IR probe was inserted through a nylon adapter and TFE O-ring seal into a Schlenk flask fitted with a magnetic stir bar. After heating the flask under vacuum and flushing it with nitrogen, a background spectrum was recorded. DMF was transferred via syringe to the IR vessel cooled to 0 °C in a thermostatted bath for 30 min. A solvent reference spectrum was recorded at 0 °C, and formamide was added at the same temperature. Following an initial period of signal stabilization, spectra were recorded every 30 s over the course of the formamide titration with a solution of MeONa (4.4 M in MeOH) at a gain of 1 and a resolution of 4 cm^{-1}.

Kinetics. A solution of methyl ester **4** containing anhydrous *o*-xylene (0.031 M) as an HPLC standard was charged to an oven-dried, nitrogen-flushed 20 mL reaction vial fitted with a TFE septum and a stir bar. The vial was brought to the desired temperature using a thermostatted bath (±0.2 °C), and the reaction was initiated by rapid injection of a stock solution of MeONa (4.4 M in MeOH) under a positive pressure of nitrogen. Aliquot portions (0.1 mL) were periodically taken and quenched with 1:1 H_2O–ACN (1 mL) at intervals chosen to ensure an adequate sampling of the first 0–15% conversion and analyzed using HPLC. The reactions were monitored by following the decay of the substrates and the formation of products relative to the internal *o*-xylene standard. Following the formation of the products afforded initial rates that were equivalent to those obtained by monitoring substrate decays within ±10%. The initial rates depicted in Figure 2 represent the average of two runs as determined using nonlinear least-squares analysis. The rates were reproducible within ±10%, and the errors reported in Supporting Information correspond to one standard deviation.

Computational Methods. All calculations were executed using Gaussian 09, revision B.01.3. A series of geometries were methodically tested for all structures at the B3LYP/6-31+G(d) level, and the lowest energy forms were submitted to single-point MP2/6-31+G(d) calculations incorporating Tomasi's polarized continuum model (PCM) corrections for formamide as the bulk solvent.[15] The calculation of solution-phase energies using gas-phase geometries has been reported previously.[27] All transition structures were reoptimized after the explicit addition of a molecule of formamide as coordinating solvent, and the resulting structures were only considered when their energies were lower than those of the unsolvated analogues.[28] The calculated energies (ΔG, 298.15 K, 1.0 atm) result from the sum of single-point MP2/6-31+G(d)//B3LYP/6-31+G(d) calculations, thermal corrections to Gibbs free energy (TCGFE) as obtained from the frequency analysis at the B3LYP/6-31+G(d) level, and PCM corrections. Energy values are given relative to the separated ester **7** and sodium formamide reactants in kcal·mol^{-1}. In the absence of structural data on the aggregation and solvation states of sodium formamide and plausible intermediates under the reaction conditions, these energies represent reactivity trends rather than precise values. Frequency calculations for all stationary points were carried out to describe them either as minima (i = 0) or as first-order transition states (i = 1). For all transition structures, visualization of the imaginary frequencies corresponded to the expected normal mode for the elementary step under investigation. Intrinsic reaction coordinate calculations (IRC) were performed from the transition states in forward and reverse directions to confirm the lowest energy reaction pathways that connect the corresponding minima.

ASSOCIATED CONTENT

Supporting Information

General methods, rate data, copies of NMR spectra, and molecular modeling coordinates. This material is available free of charge via the Internet at http://pubs.acs.org.

AUTHOR INFORMATION

Corresponding Author

*E-mail: antonio.ramirez1@bms.com.

■ ACKNOWLEDGMENTS

We thank David Kronenthal, Robert Waltermire, Francisco González-Bobes, Lopa Desai, Peng Geng, Jing Liang, and Annie Tam for helpful discussions during the preparation of the manuscript. We also acknowledge the analytical support provided by Jingpin Jia, Jonathan Marshall, Curtis Tinker, and Alice Yang during the development of this work.

■ REFERENCES

(1) For recent examples, see: (a) Abrecht, S.; Adam, J.-M.; Bromberger, U.; Diodone, R.; Fettes, A.; Fischer, R.; Goeckel, V.; Hildbrand, S.; Moine, G.; Weber, M. *Org. Process Res. Dev.* **2011**, *15*, 503−514. (b) Giubellina, N.; Stabile, P.; Laval, G.; Perboni, A. D.; Cimarosti, Z.; Westerduin, P.; Cooke, J. W. G. *Org. Process Res. Dev.* **2010**, *14*, 859−867. (c) Wagner, J.; von Matt, P.; Sedrani, R.; Albert, R.; Cooke, N.; Ehrhardt, C.; Geiser, M.; Rummel, G.; Stark, W.; Strauss, A.; Cowan-Jacob, S. W.; Beerli, C.; Weckbecker, G.; Evenou, J.-P.; Zenke, G.; Cottens, S. *J. Med. Chem.* **2009**, *52*, 6193−6196. (d) Scott, D. A.; Bell, K. J.; Campbell, C. T.; Cook, D. J.; Dakin, L. A.; Del Valle, D. J.; Drew, L.; Gero, T. W.; Hattersley, M. M.; Omer, C. A.; Tyurin, B.; Zheng, X. *Bioorg. Med. Chem. Lett.* **2009**, *19*, 701−705.

(2) (a) Voets, M.; Antes, I.; Scherer, C.; Müller-Vieira, U.; Biemel, K.; Barassin, C.; Marchais-Oberwinkler, S.; Hartmann, R. W. *J. Med. Chem.* **2005**, *48*, 6632−6642. (b) DeRoy, P. L.; Charette, A. B. *Org. Lett.* **2003**, *5*, 4163−5165. (c) Homan, E. V.; Tulp, M.; Th., M.; Nilsson, J. E.; Wikström, H. V.; Grol, C. J. *Bioorg. Med. Chem. Lett.* **1999**, *7*, 2541−2548. (d) Weisz, I.; Roboz, J.; Wolf, I.; Szabo, J.; Beke, J. G. *Bioorg. Med. Chem. Lett.* **1998**, *8*, 3241−3244. (e) Deo, N. M.; Crooks, P. A. *Synth. Commun.* **1995**, *25*, 691−701.

(3) Allred, E. L.; Hurwitz, M. D. *J. Org. Chem.* **1965**, *30*, 2376−2381.

(4) (a) Pinto, D.; Quan, M.; Orwat, M.; Li, Y.-L.; Han, W.; Qiao, J.; Lam, P.; Koch, S. Preparation of Heteroaryllactams as Factor Xa Inhibitors. PCT Int. Appl. WO 2003036652 A1. (b) Shapiro, R.; Rossano, L. T.; Mudryk, B. M.; Cuniere, N.; Oberholzer, M.; Zhang, H.; Chen, B.-C. Process for Efficient Preparation of 4,5-Dihydropyrazolo[3,4-*c*]pyridine-2-one Derivatives. U.S. Patent Appl. 20060069258 A1. (c) Pinto, D. J. P.; Orwat, M. J.; Koch, S.; Rossi, K. A.; Alexander, R. S.; Smallwood, A.; Wong, P. C.; Rendina, A. R.; Luettgen, J. M.; Knabb, R. M.; He, K.; Xin, B.; Wexler, R. R.; Lam, P. Y. S. *J. Med. Chem.* **2007**, *50*, 5339−5356. (d) Bates, S. M.; Weitz, J. I. *Drugs Future* **2008**, *33*, 293−301. (e) Galanis, T.; Thomson, L.; Palladino, M.; Merli, G. J. *J. Thromb. Thrombolysis* **2011**, *31*, 310−320. (f) Maxwell, B. D.; Tran, S. B.; Chen, S.-Y.; Zhang, D.; Chen, B.-C.; Zhang, H.; Bonacorsi, S. J. Jr. *J. Labelled Compd. Radiopharm.* **2011**, *54*, 418−425.

(5) The actual process for the preparation of carboxamide **6** involves amidation of the ethyl ester analogue of **4** with formamide and MeONa. Under the reaction conditions, transesterification to the methyl ester **4** is virtually instantaneous. Details for the preparation and characterization of carboxamide **6** have been reported previously.[4c,f]

(6) For a mechanistic study on the NaOH-mediated deprotonation of formamide, see: Rodriquez, C. F.; Guo, X.; Shoeib, T.; Hopkinson, A. C.; Siu, K. W. M. *J. Am. Soc. Mass Spectrom.* **2000**, *11*, 967−975.

(7) (a) Correa, N. M.; Pires, P. A. R.; Silber, J. J.; El Seoud, O. A. *J. Phys. Chem. B* **2005**, *109*, 21209−21219. (b) Nast, R.; Dilly, P. *Angew. Chem., Int. Ed. Engl.* **1967**, *6*, 357. (c) Evans, J. C. *J. Chem. Phys.* **1954**, *22*, 1228−1234.

(8) The deprotonation of formamide-d_3 under identical conditions was also instantaneous.

(9) Formamide is a stronger acid than MeOH: (a) Marlier, J. F.; Campbell, E.; Lai, C.; Weber, M.; Reinhardt, L. A.; Cleland, W. W. *J. Org. Chem.* **2006**, *71*, 3829−3836. (b) Hine, J.; Hine, M. *J. Am. Chem. Soc.* **1952**, *74*, 5266−5271.

(10) Monitoring the amidation by ^{13}C NMR confirmed the formation of sodium diformylamide; see Supporting Information.

(11) Espenson, J. H. In *Chemical Kinetics and Reaction Mechanisms*; McGraw-Hill: New York, 1995; pp 7−81.

(12) The protonated form of intermediate **5** was identified by LCMS analysis from reaction mixtures. Its structure was corroborated by comparison with the independently synthesized material.

(13) Analysis of the initial rates between −20 and 20 °C provides an activation energy E_a = 16 ± 1 kcal/mol in line with related hydrolyses of aromatic methyl esters: Mitton, C. J.; Schowen, R. L.; Gresser, M.; Shapley, J. *J. Am. Chem. Soc.* **1969**, *91*, 2036−2044.

(14) Rate data and parameters for the Hammett plot are archived in Supporting Information. For a discussion of related Hammett plots on ester aminolyses, see: Knowlton, R. C.; Byers, L. D. *J. Org. Chem.* **1988**, *53*, 3862−3865, and references cited therein.

(15) (a) Mennucci, B.; Cammi, R., Eds.; *Continuum Solvation Models in Chemical Physics. From Theory to Applications*; John Wiley & Sons: Chichester, UK, 2007. (b) See the Supporting Information for details and references.

(16) Ramirez, A.; Lobkovsky, E.; Collum, D. B. *J. Am. Chem. Soc.* **2003**, *125*, 15376−15387.

(17) For a review on the competing pathways for the collapse of tetrahedral intermediates akin to **8**, see: Stirling, C. M. *Acc. Chem. Res.* **1979**, *12*, 198−203.

(18) Unconstrained searches for the elimination of MeONa failed to converge. An alternative relaxed-scan approximation by lengthening the C(O)−O bond affords a flat potential energy surface associated with structures that display MP2 dissociation energies ∼26 kcal/mol.

(19) For a discussion on solvent assistance in the reverse process, the basic methanolysis of amides, see: (a) Šktrajbl, M.; Florián, J.; Warshel, A. *J. Am. Chem. Soc.* **2000**, *122*, 5354−5366. (b) Venkatasubban, K. S.; Schowen, R. L. *J. Org. Chem.* **1984**, *49*, 653−655. (c) Broxton, T. J.; Deady, L. W. *J. Org. Chem.* **1975**, *20*, 2906−2910.

(20) Bordwell, F. G. *Acc. Chem. Res.* **1988**, *21*, 456−463.

(21) For studies on related 1,3-proton shifts in the aminolysis of esters, see: Galabov, B.; Atanasov, Y.; Ilieva, S.; Schaefer, H. F. *J. Phys. Chem. A* **2005**, *109*, 11470−11474, and references cited therein.

(22) Kamiya, K.; Boero, M.; Shiraishi, K.; Oshiyama, A. *J. Phys. Chem. B* **2006**, *110*, 4443−4450.

(23) The rate law provides the stoichiometry of the rate-determining transition structure relative to the reactants: (a) McNeil, A. J.; Ramirez, A.; Collum, D. B. *Angew. Chem., Int. Ed.* **2007**, *46*, 3002−3017. (b) Edwards, J. O.; Greene, E. F.; Ross, J. *J. Chem. Educ.* **1968**, *45*, 381−385.

(24) (a) Sakamoto, I. *Jpn Anal.* **1990**, *39*, 333−340. (b) Parker, A. J. *Pure Appl. Chem.* **1981**, *53*, 1437−1445. (c) Cox, B. G.; Hedwig, G. R.; Parker, A. J.; Watts, D. W. *Aust. J. Chem.* **1974**, *27*, 477−501. (d) Greenberg, M. S.; Bodner, R. L.; Popov, A. I. *J. Phys. Chem.* **1973**, *77*, 2449−2454.

(25) Burt, J. L.; Braem, A.; Ramirez, A.; Mudryk, B.; Rossano, L.; Tummala, S. *J. Pharm. Innov.* **2011**, *6*, 181−192.

(26) Bunnett, J. F.; Davis, G. T.; Tanida, H. *J. Am. Chem. Soc.* **1962**, *84*, 1606−1614.

(27) (a) Rousseaux, S.; Gorelsky, S. I.; Chung, B. K. W.; Fagnou, K. *J. Am. Chem. Soc.* **2010**, *132*, 10692−10705. (b) Wheeler, S. E.; McNeil, A. J.; Müller, P.; Swager, T. M.; Houk, K. N. *J. Am. Chem. Soc.* **2010**, *132*, 3304−3311.

(28) Molecular coordinates of high energy structures with alternative solvation and connectivites not referred to herein for brevity are available upon request.